JOURNAL OF MATERIALS SCIENCE 32 (1997) 289–294

Effect of magnesium alloying additions on infiltration threshold pressure and structure of SiC powder compacts infiltrated by aluminium-based melts

E. CANDAN, H. V. ATKINSON, H. JONES
Department of Engineering Materials, University of Sheffield, Mappin Street, Sheffield, S1 3JD, UK

Infiltration of 53% dense preforms of 23 μm size SiC particulate by Al–0 to 14 wt % Mg alloy melts has been carried out at different applied pressures at 750 °C, together with microstructural characterization of the resulting composites. The threshold pressure P^* for infiltration decreased with increasing Mg content in the melt at twice the rate by which its surface tension decreased, the residual effect being attributable to the expected effect of Mg on the contact angle between Al and SiC. Periodic bands of entrapped porosity at lower Mg contents and infiltration pressures just above P^* are thought to have arisen from periodic arrest of the infiltration front pending ventilation of the gas accumulated at the front. The formation of monolithic Mg_2Si and areas of lamellar αAl–Mg_2Si eutectic observed at higher Mg contents is associated with the accumulation of 5 wt % Si in the melt as a result of reaction between the melt and SiC.

1. Introduction

The production of metal matrix composites (MMCs) by infiltration of the molten matrix into a preheated ceramic preform followed by solidification continues to attract widespread interest and attention which has been recently reviewed [1, 2]. A previous paper [3] reported the effect of ceramic particle size, melt superheat, impurities and single or combined alloy additions on threshold pressure P^* for infiltration of SiC particle compacts by Al-based melts. The addition of 0.5 wt % Mg to a 99.9 wt % Al melt was found to have little effect on P^* while addition of a further 1 wt % Mg to a 2014 Al alloy did significantly reduce P^*. The present objective is to explore the effects of Mg additions over a wider range of concentrations, including their effects on the structural characteristics of the resulting MMCs.

2. Experimental procedures

The SiC for the compacts was the F360 size range (average particle size 22.8 μm) supplied by Abrafact Ltd for the previous work. Compacts of diameter 10.4 mm and length 42 mm were prepared as in the previous study to give a void fraction of 0.47 ± 0.005 in the compact. Matrix alloys containing 1–14 wt % Mg were made by melting together 99.95% pure Al and 99.7% pure Mg in graphite crucibles and chill casting as 25 mm diameter ingots. The infiltration system was essentially that described previously, except that the bulkhead union used to fix the sample holder to the connecting tube was replaced by an 'O' ringed stainless steel adapter located adjacent to the lid of the infiltration vessel (Fig. 1(a–c)). Another difference was that the aluminium cap used previously to close the lower end of the silica tube containing the compact was replaced by a porous alumina filter. This filter was 10 mm in diameter and 5 mm long and contained 85% porosity, offering negligible resistance to flow of the alloy melt into the SiC compact. Infiltration was carried out at 750 ± 5 °C, with the compact immersed in the melt, by increasing the pressure of nitrogen in the containment vessel at 20 psi (140 kPa) s^{-1} to a predetermined value, holding it for 2 min, then decreasing it at 30 psi (210 kPa) s^{-1}. The infiltration distance was determined as a function of applied pressure P from longitudinal slices of resulting solidified compacts. The same longitudinal sections were used to determine the location of residual porosity and matrix microstructure, after metallographic polishing to a 0.25 μm finish.

3. Results

Fig. 2 shows infiltration distance versus applied pressure for 99.95% Al and the five Al-Mg alloy compositions studied. The resulting threshold pressures P^* are given as a function of Mg alloying content in Table 1, with corresponding values $W_i\lambda = \frac{1}{6}(\frac{1}{f} - 1)\, P^* d$ where W_i is the work of immersion, λ is a particle shape factor (> 1 for nonspherical particles), f is the particle

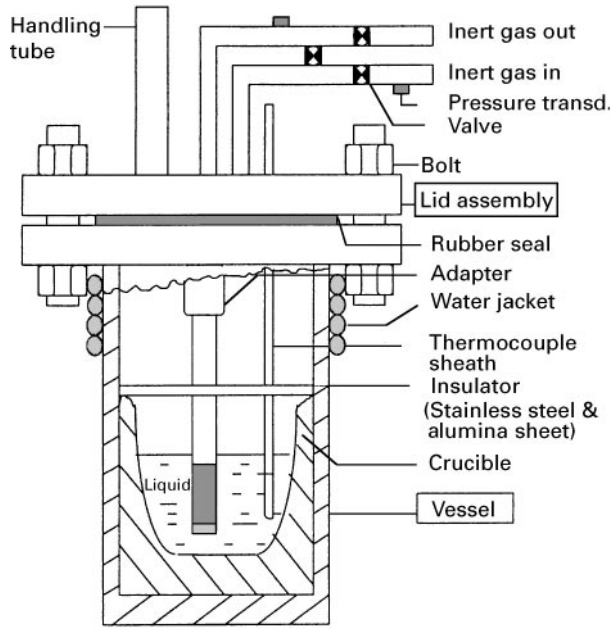

(a)

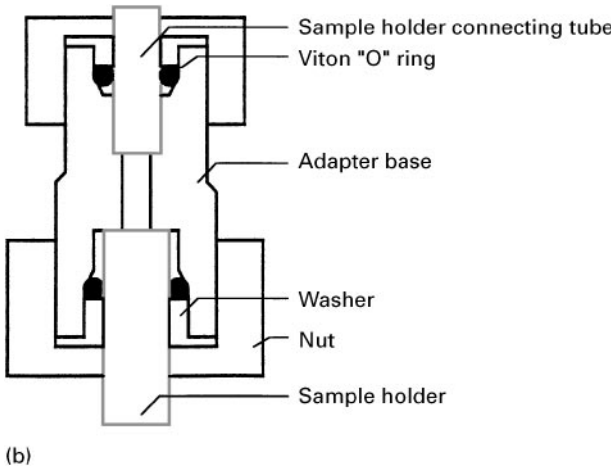

(b)

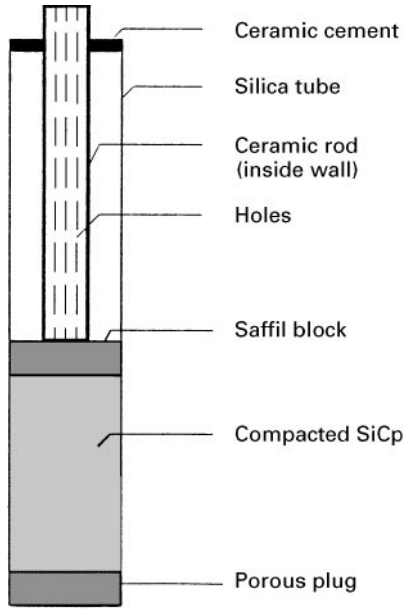

(c)

Figure 1 System for infiltration: (a) general schematic, (b) detail of adapter, (c) configuration of sample holder.

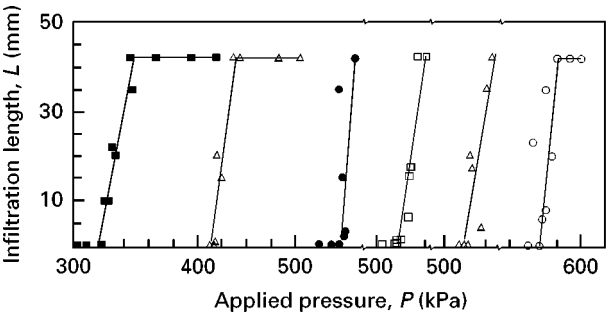

Figure 2 Infiltration distance versus applied pressure for infiltration of Al–Mg alloy melts into SiC_p compacts: Key to symbols; (○) 0, (△) 1.0, (□) 1.7, (●) 3.4, (△) 8.6 and (■) 13.9 wt% Mg.

TABLE I Threshold presssure P^* for infiltration versus Mg alloying content from Fig. 2 and derived $W_i\lambda$

Mg-content, (wt%)	O	1.0	1.7	3.4	8.6	13.9
P^* (kPa)	565	533	522	518	411	320
$W_i\lambda$ (N m^{-1})	1.9	1.8	1.8	1.8	1.4	1.1

volume fraction and d is the particle size. Longitudinal sections of samples infiltrated at pressures that gave an infiltration distance of 35–40 mm in 2 min showed the features evident in Fig. 3(a–f). The periodic dark banded features in the pure Al and Al–1.0, 1.7 and 3.4 wt % Mg samples were associated with porosity (Fig. 4a) while the more uniformly distributed dark features in Al–8.6 and 13.9 wt % Mg were associated with concentrations of Mg_2Si (Fig. 4b) formed by chemical reaction between SiC and the melt. This latter effect was evidently more pronounced in the initial than the final part of the Al–13.9 wt % Mg sample whereas the initial part was free of it for Al–8.6 wt % Mg. Reaction products were also evident at SiC surfaces even where such relatively massive Mg_2Si had not formed (Fig. 5(a–c)). The alloy matrix was otherwise metallographically featureless except for two-phase eutectic-like areas in the Al–8.6 and 13.9 wt % Mg samples (Fig. 5(b and c)). XRD (Fig. 6) indicates the presence of Al_4C_3 and Si in the infiltrated samples, together with Mg_2Si from the alloy matrices, in addition to αAl and SiC.

4. Discussion

The tendency for threshold pressure P^* and associated $W_i\lambda$ to decrease with increasing Mg alloying content C_o in the melt (Table 1) is in full accord with previously reported results for this system [3–6]. The most helpful comparison is afforded by plotting $W_i\lambda$ versus Mg-content as in Fig. 7. Previous results [5, 6] for infiltration at 750 °C are in reasonable correspondence with our results, also for 750 °C, which extend the results of references [5, 6] to much higher Mg-contents. The two sets of results reported in references [3, 4] for 800 °C are also in good mutual agreement for the small range of Mg-content investigated. The mean slope $d(W_i\lambda)/dC$ is ~ 0.06 N m^{-1} per wt % Mg

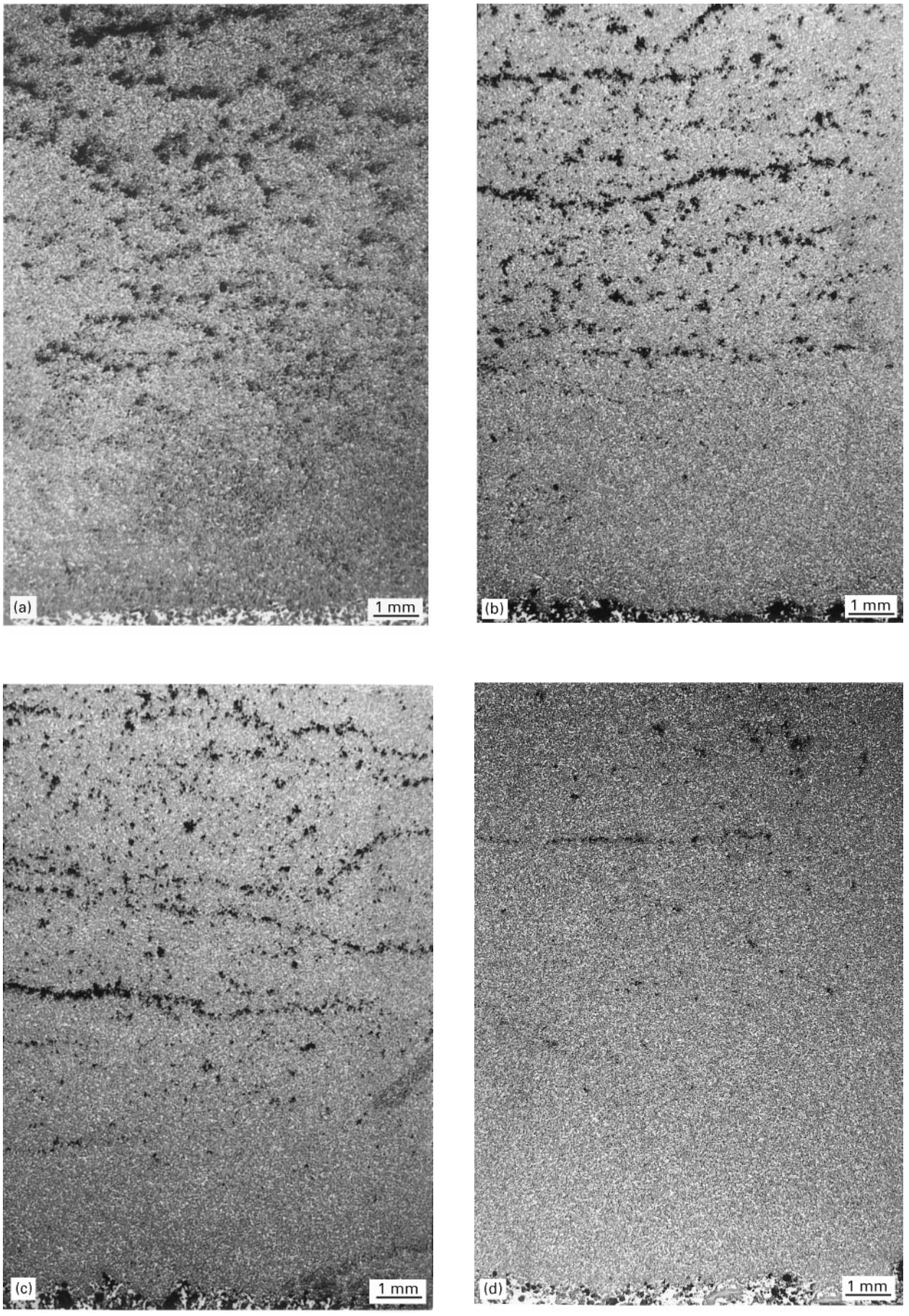

Figure 3 Optical micrographs of longitudinal sections of SiC infiltrated with Al (a) O, (b) 1.0, (c) 1.7, (d) 3.4, (e) 8.6 and (f) 13.9 wt % Mg.

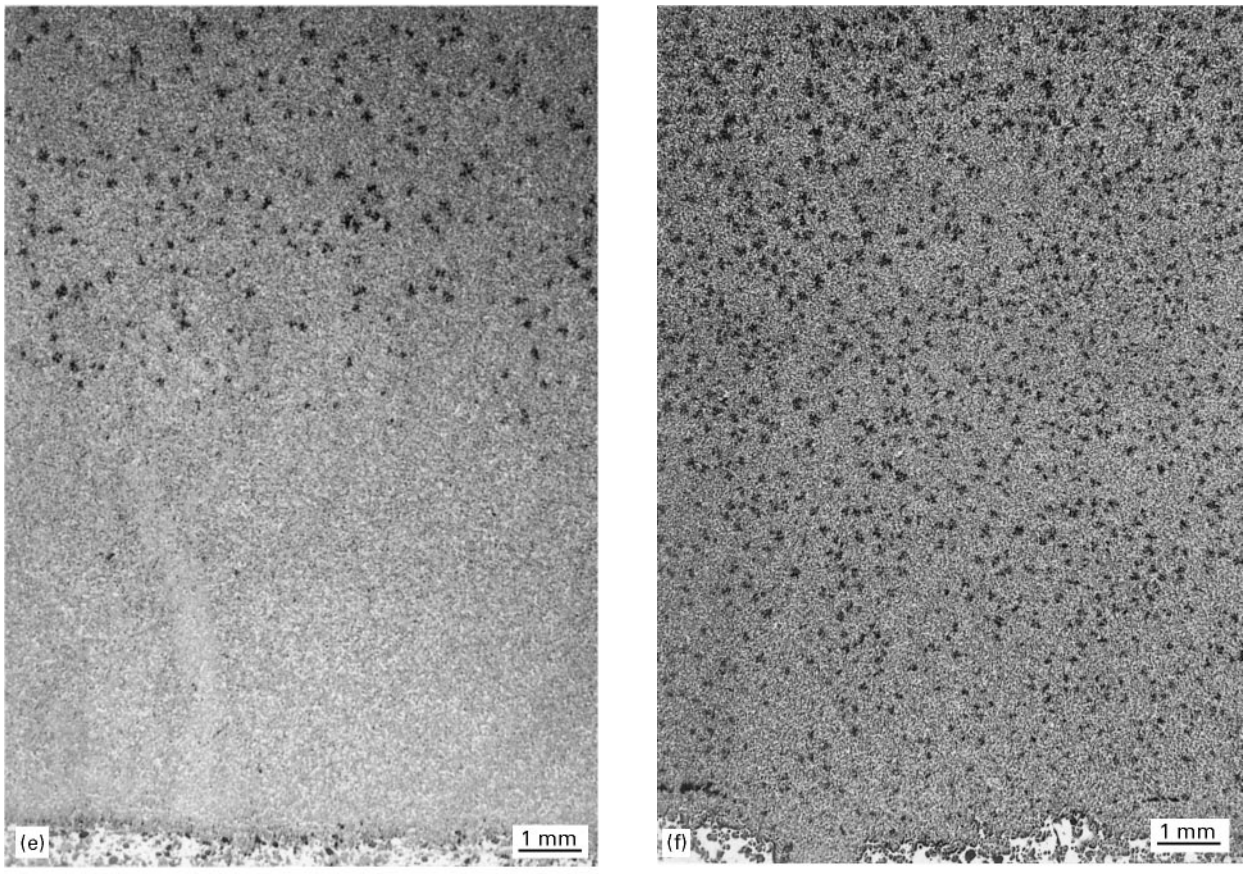

Figure 3 (continued)

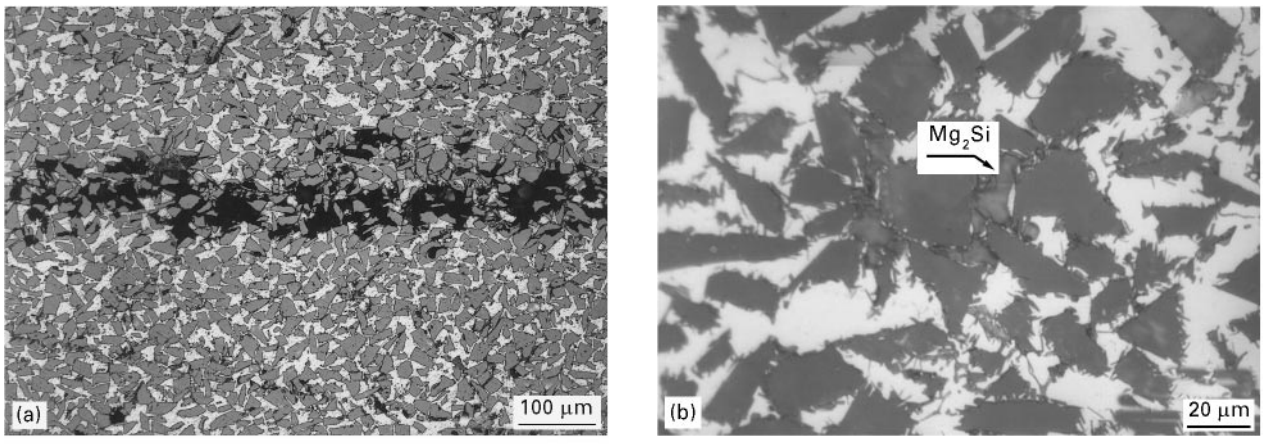

Figure 4 (a) Optical micrograph showing (a) nature of banded porosity in Al–3.4 wt % Mg and (b) SEM micrograph showing clustered product of reaction between SiC and the melt for Al–8.6 wt % Mg, identified by XRD and SEM microanalysis as Mg_2Si.

for both infiltration temperatures, though values of $W_i\lambda$ are doubled for infiltration at 750 °C compared with 800 °C, at least over the range 0–5 wt % Mg for which measurements are available. W_i is normally identified with $\gamma_L \cos\theta$ where γ_L is the surface tension of the liquid and θ is the equilibrium contact angle between the liquid and infiltrated solid [2, 4, 6]. Published data [7–10] indicate decreases in the surface tension γ_L with an increase of Mg-content in Al–Mg alloy melts. At 700 °C, γ_L reportedly [10] decreases from 1.12 to 1.02 N m^{-1} with the addition of 8 wt% Mg to Al for an unoxidized surface (from 0.87 to 0.78 N m^{-1} for an oxidized surface). Such 10% decreases at 700 °C are smaller than the $>20\%$ decreases in $W_i\lambda$ indicated in Fig. 7 for an 8 wt % Mg addition at 750 or 800 °C. The contact angle θ between pure aluminium and single crystal [11] or sintered [12] SiC is $\sim$150 or 130° at 700 °C in vacuum. The lower value of $\sim$100° for reaction bonded SiC is reduced by some 35° on the addition of 5 wt % Mg to

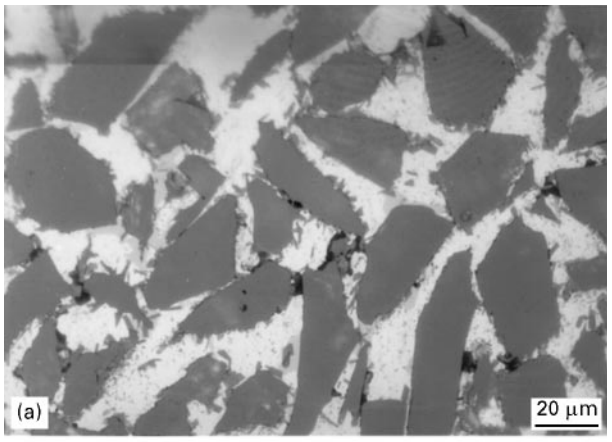

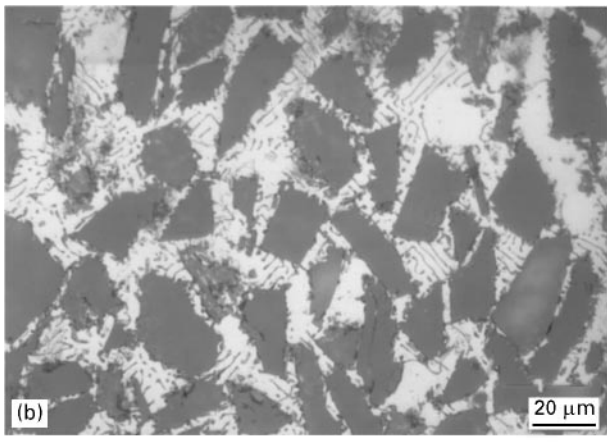

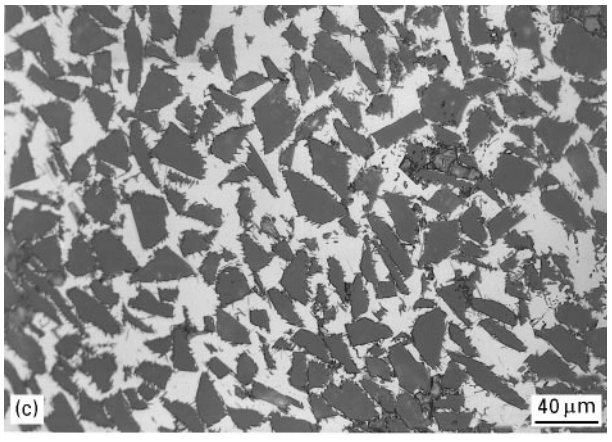

Figure 5 Optical micrographs showing typical interaction products at the surface of SiC particles for (a) Al–3.4 wt% Mg, (b) Al–8.6 wt% Mg and (c) Al–13.9 wt % Mg towards the bottom of the infiltrated compact.

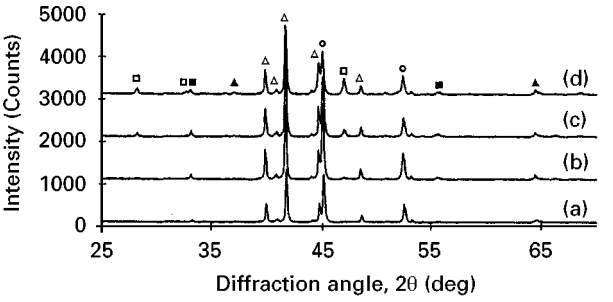

Figure 6 X-ray diffraction patterns for SiC infiltrated with (a) Al–0, (b) 3.4, (c) 8.6 and (d) 13.9 wt % Mg. Key: (○) αAl, (△) SiC, (□) Mg_2Si, (▲) Al_4C_3 (■) Si.

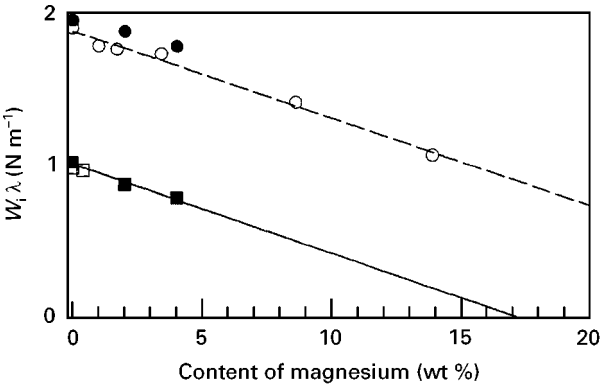

Figure 7 Product of work of immersion W_i and particle shape factor λ versus Mg content in Al–Mg alloy melts pressure infiltrated into SiC particle compacts. (■) Oh *et al.* [4], (□) Chong *et al.* [3], (●) Alonso *et al.* [5, 6], (○) Present work. Melt temperatures: (■ □) 800 °C; (● ○) 750 °C. The full line represents $W_i\lambda = -0.0572C_0 + 1.00$ whilst the dashed line represents $W_i\lambda = -0.0562\,C_0 + 1.88$ where C_0 is the Mg content of the melt.

the melt [13]. The 10% reduction in cos θ on the addition of 8 wt% Mg implied by our results would require an applicable θ value of say 140° for pure Al to be reduced by less than 10°.

The periodic bands of porosity found in the pure Al and 1.0, 1.7 and 3.4 wt % Mg samples do not seem to have been previously reported for pressure infiltrated ceramic preforms. All these infiltrations were produced at infiltration pressures barely above the threshold pressure P^* so that the infiltration front did not advance beyond the end of the preform. These bands of porosity were eliminated when the infiltration pressure was raised sufficiently for infiltration to extend beyond the preform. The periodic effect at just above P^* may be associated with accumulation and compression of displaced gas ahead of the advancing infiltration front to a level at which advance is arrested momentarily to allow accumulated gas to vent from the top of the preform, leaving unfilled pockets of gas when infiltration restarts at vulnerable points on the arrested front. Such effects have been reported in the 1940's [14, 15] for the infiltration of soils by moisture and have been associated subsequently with periodic fluctuations of gas pressure, escape of gas bubbles and appearance of tongue flow in bounded columns of such infiltrated particulates [16–20].

The concentrations of monolithic Mg_2Si found in the Al–8.6 and 13.9 wt % Mg indicate that pick-up of silicon by the melt as a result of reaction with the SiC exceeded levels equivalent to that necessary to form the pseudobinary αAl–Mg_2Si eutectic with a reported eutectic temperature 595 °C and composition of 8.15 wt % Mg, 4.75 wt % Si [21, 22]. This composition is entirely consistent with the extensive areas of lamellar eutectic found in the Al–8.6 wt % Mg sample.

5. Conclusions

(1) The threshold pressure P^* for melt infiltration of 53% dense preforms of 23 μm SiC particulate decreased from 570 to 320 kPa on addition of 13.9 wt % Mg to a pure aluminium melt. Part of this decrease appears to be attributable to the known effect of Mg on the surface tension of liquid aluminium, the remainder probably stemming from the effect of Mg in reducing the contact angle between the melt and SiC.

(2) Periodic bands of entrapped porosity found at lower melt concentrations of Mg and infiltration pressures just above P^* may be associated with periodic arrest of the advancing infiltration front by accumulation there of displaced gas, to allow venting of this from the end of the compact.

(3) Formation of monolithic Mg_2Si in Al–8.6 and 13.9 wt % Mg/SiC_p samples and of extensive lamellar αAl–Mg_2Si eutectic areas in Al–8.6 wt % Mg/SiC_p is consistent with pick-up of some 3.4 wt % Si by the melt as a result of reaction with the SiC during and following infiltration.

Acknowledgements

This work formed part of a PhD programme at the University of Sheffield supported by a scholarship for EC from the Turkish Government.

References

1. R. ASTHANA, P. K. ROHATGI and S. N. TEWARI, *Proc. Adv. Mater.* **2** (1992) 1.
2. R. MORTENSEN, V. J. MICHAUD and M. C. FLEMINGS, *J. Metals* **45** (1993) 36.
3. S. Y. CHONG, H. V. ATKINSON and H. JONES, *Mater. Sci. Engng. A* **A173** (1993) 233.
4. S.-Y. OH, J. A. CORNIE and K. C. RUSSELL, *Met. Trans. A* **20A** (1989) 533.
5. A. ALONSO, A. DAVIES, J. NARCISO, C. GARCIA-CORDOVILLA and E. LOUIS, Proc. ICCM9, Madrid, July 1993, edited by A. Miravete, (Woodhead Publ. Ltd, Abington, UK, 1993) Vol. 1, pp. 187–194.
6. J. NARCISO, A. ALONSO, A. PAMIES, C. GARCIA-CORDOVILLA and E. LOUIS, *Scripta Met. Mater.* **31** (1994) 1495.
7. E. GEBHARDT, E. M. BECKER and S. DORNER, *Z. Metallkunde* **45** (1954) 83.
8. A. M. KOROLKOV, *Izv. Akad. Nauk. SSSR, Otdel Tekh Nauk* **2** (1956) 35.
9. *idem*, in "Casting Properties of Metals and Alloys", (Con. Bur, New York, 1963) Ch. 3.
10. C. GARCIA-CORDOVILLA, E. LOUIS and A. PAMIES, *J. Mater. Sci.* **21** (1986) 2787.
11. W. KÖHLER, *Aluminium* **51** (1975) 443.
12. M. SHIMBO, M. NAKA and I. OKAMOTO, *J. Mater. Sci. Lett.* **8** (1989) 663.
13. D.-S. HAN, H. JONES and H. V. ATKINSON, *J. Mater. Sci.* **28** (1993) 2654.
14. R. E. HORTON, *Soil Sci. Soc. Am. Proc.* **5** (1940) 399.
15. J. E. CHRISTIANSEN, *Soil Science* **58** (1944) 355.
16. L. G. WILSON and J. N. LUTHIN, *ibid* **91** (1963) 137.
17. E. G. YOUNGS and A. J. PECK, *ibid*, **98** (1964) 290.
18. A. J. PECK, *ibid* **99** (1965) 327.
19. *Idem*, *ibid* **100** (1965) 44.
20. Z. WANG and J. FEYEN, in "Unsaturated Soils", edited by E. E. Alonso and P. Delage Vol. 1 (A. A. Balkema, Rotterdam, 1995) pp. 417–422.
21. E. H. DIX, F. KELLER and R. W. GRAHAM, *Trans. AIMME* **93** (1931) 404.
22. H. W. L. PHILLIPS, *J. Inst. Met.* **72** (1946) 151.

Received 13 May
and accepted 2 July 1996